J. Electrochem. Sci. Eng. **15(2)** (2025) 2512 http://dx.doi.org/10.5599/jese.2512

Open Access : : ISSN 1847-9286
https://pub.iapchem.org/ojs/index.php/JESE

Original scientific paper

A new potential of sodium anthraquinone-2-sulfonate as a corrosion inhibitor for carbon steel in 0.5 M H_2SO_4

Roza Kenzhegalieva, Meruyet Khapiyeva, Gauhar Uzakbay, Aruzhan Talapova, Ruben Vardanyan and Nikolay Akatyev✉

Makhambet Utemisov West Kazakhstan University, N. Nazarbayev Ave. 162, Uralsk 090000, The Republic of Kazakhstan

Corresponding authors: ✉nikolay.akatyev@wku.edu.kz

Received: September 21, 2024; Accepted: January 14, 2025; Published: January 22, 2025

Abstract

The present study investigates the inhibitory properties of sodium anthraquinone-2-sulfonate (AQ2SNa). Weight loss measurements, electrochemical tests, and metal surface analysis were carried out in this study to evaluate the adsorption behavior of the compound and its influence on the corrosion rate of carbon steel in 0.5 mol dm^{-3} H_2SO_4 solution. Density functional theory DFT/B3LYP/6-311+G(d,p) and molecular dynamic simulation (MD) were applied for theoretical studies to evaluate the inhibiting effect and understand the mechanism of interaction of inhibitor molecules with Fe (110) surface. It was found that the inhibition efficiency of AQ2SNa in 0.5 mol dm^{-3} H_2SO_4 solution reached up to 94.44 % at the maximum concentration (0.5 g dm^{-3}). Thermodynamic parameters show that the adsorption process is spontaneous and endothermic, suggesting the conformance of strong interactions between inhibitor and metal surface according to the Langmuir adsorption model. The spontaneous physisorption (ΔG^0_{ads} > -20 kJ mol^{-1}) of the inhibitor molecules led to high efficiency. Analysis of dynamic polarization curves showed that AQ2SNa acts as an inhibitor of a mixed nature. The results also indicate that AQ2SNa significantly increases the contact angle, indicating increased hydrophobicity due to the formation of a stable film on the metal surface. Theoretical parameters were compared to experimental data. The results highlight the novel potential of AQ2SNa as an effective corrosion inhibitor to provide an effective solution for enhancing the protection of carbon steel in acidic media.

Keywords

Organic corrosion inhibitors; metal protection; weight loss; electrochemical tests, quantum chemical calculations

Introduction

Corrosion poses a significant challenge to various industries as the deterioration of metals and alloys can lead to structural failures, reduced efficiency and significant economic losses [1]. The

addition of corrosion inhibitors is still the most effective way of preventing metal corrosion. To prevent the corrosive destruction of metals, individual compounds of various nature (organic, inorganic) and origin (synthetic, natural), comprising mixed compositions [2], polymers and their composites [3], or extracts obtained from natural sources (plant [4], biomass [5]) or plant waste [6,7], can be used. Corrosion inhibitors adsorb onto the metal surface, forming a protective film that prevents corrosive agents from reaching the metal. This adsorption can be physical (physisorption) or chemical (chemisorption). The protective layer can be composed of oxides or other less reactive compounds than the base metal [8].

Anthraquinones form a large and diverse subgroup within the quinone superfamily. The first study of the effect of anthraquinone and some of its derivatives on the corrosion resistance of metals in sulfuric acid solution was published in 1969 by Kuzyukov and Levin [9]. Three amide derivatives of 1-aminoanthraquinones synthesized from long chain fatty acids were investigated by Muthukumar as effective corrosion inhibitors. It has been shown that the inhibitory effectiveness of these compounds can reach 84 % [10]. Saqalli *et al.* [11] reported the influence of hydroxyl group number of some anthraquinone derivatives 1,2,4-trihydroxyanthraquinone (purpurin) and 1,4-dihydroxyanthraquinone (quinizarin) on their corrosion inhibition efficiency. Electrochemical studies and quantum chemical calculations revealed that the compound containing supplementary group (OH) presents the highest inhibition efficiency (91.5 %). The anticorrosive properties of alizarin (also a hydroxy derivative of anthraquinone) as a cathodic inhibitor of mild steel corrosion in 1.0 M HCl solution are well known [12]. Furthermore, Bensouda *et al.* demonstrated that *Mentha piperita* essential oil, containing 1-(p-fluorophenyl) anthraquinone as the main component (42.8 %), showed an inhibitory effect of up to 87 % for mild steel in HCl solution [13].

Sodium anthraquinone-2-sulfonate (AQ2SNa, Figure 1) is a water-soluble anthraquinone derivative that can be prepared by sulfonation of anthraquinone.

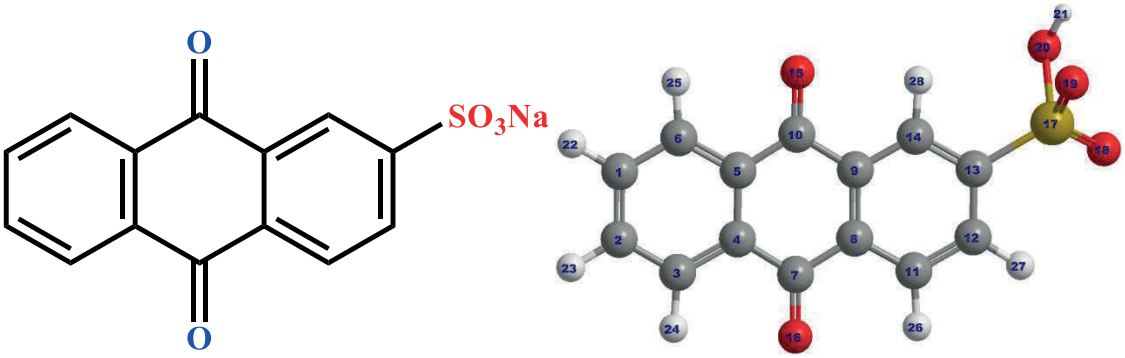

Figure 1. *Chemical structure and ball-and-stick model of AQ2SNa with atomic enumeration*

Nowadays, the AQ2SNa has a wide range of applications. It is used in high-performance supercapacitors [14], in photochemistry [15], as a co-catalyst [16], and for developing nano-antibacterial materials [17] and multifunctional sensors [18]. Articles dealing with anti-corrosion properties of AQ2SNa are exclusively concerned with the use of AQ2SNa as a self-deoxidizing additive to an electrolyte of aqueous-zinc batteries to prevent zinc anode corrosion and dendrite growth [19]. In related studies, sulfonate-rich layers have been shown to modulate ion transport at the anode-electrolyte interface. These layers create electrostatic repulsion that blocks harmful species from reaching the zinc surface while facilitating the desolvation of zinc ions. This mechanism helps in reducing undesirable side reactions and promotes uniform zinc deposition [20]. Nevertheless, nowadays, there is no information on using AQ2SNa as a corrosion inhibitor of other metals in liquid media or against any other type of corrosion.

Therefore, the aim of the present study is to investigate the corrosion protection properties of AQ2SNa for carbon steel in acidic media.

Experimental

Materials and solution

A freshly prepared corrosive medium comprising 0.5 mol dm^{-3} sulfuric acid (H_2SO_4) solution obtained by diluting high-grade concentrated sulfuric acid (98.3 %) with double distilled water (DDW) was utilized in this study. The corrosion inhibitor was incorporated into the solution at concentrations spanning 0.05, 0.1, 0.2, 0.3, 0.4 and 0.5 g dm^{-3}. Analytical grade (≥ 98 %) AQ2SNa as a monohydrate was purchased from commercial suppliers and used without further purification.

Sample preparation

Carbon steel specimens containing 97.8 wt.% Fe, 0.22 wt.% C, 0.65 wt.% Mn, 0.30 wt.% Si, 0.04 wt.% P, 0.05 wt.% S, 0.30 wt.% Cr, 0.30 wt.% Ni, 0.30 wt.% Cu and 0.01 wt.% N, with dimensions of 25.0×35.0×3.0 mm, were acquired from the industrial sector for corrosion testing. Before the experiment, the samples were polished in sequence using emery paper with grit numbers between 250 and 1200. The specimens were washed in running water and DDW to remove oxides and dust and then cleaned and degreased with ethanol and acetone. The specimens were prepared and kept in a desiccator with silica gel until the upcoming corrosion tests.

Weight loss (gravimetric) measurements

The weight loss experiments were performed to evaluate the corrosion rate (CR), degree of surface coverage (θ), and inhibition efficiency (IE). Every sample was placed in a beaker preliminarily filled with 100 ml of corrosion medium at room temperature. Samples were removed from the beaker following the soaking time and gently scrubbed with a soft brush under tap water and DDW. Then, they were immersed in a mixture of 50 % NaOH and 100 g of zinc dust [21] to remove any leftover corrosion product residues. Before being reweighted, the samples were rewashed in tap water and DDW, followed by rinsing in ethanol, acetone, and drying. The Ohaus Adventurer Pro AV264 analytical balance was utilized for all weighing tasks with a precision of ±0.1mg.

Equations (1) to (3) were employed for the determination of the corrosion rate (CR / g m^{-2} h^{-1}), inhibition efficiency (IE / %), and degree of surface coverage (θ), respectively:

$$CR = \frac{\Delta m}{S\tau} \quad (1)$$

$$IE = \frac{CR_0 - CR_i}{CR_0} 100 \quad (2)$$

$$\theta = \frac{IE}{100} \quad (3)$$

where Δm / g is the weight loss of the carbon steel specimen after the immersion time τ / h, S / m^2 is the surface area of the carbon steel specimen, CR_0 is the corrosion rate of carbon steel without inhibitor, and CR_i is the corrosion rate of carbon steel with the addition of inhibitor.

Activation parameters calculations

The activation energy was determined in accordance with the logarithmic form of the Arrhenius Equation (4) as follows:

$$\log \mathrm{CR} = \log A - \frac{E_a}{2.303\,RT} \quad (4)$$

where A is the Arrhenius pre-exponential factor, T / K is absolute temperature, and R is the universal gas constant (8.314 J mol^{-1} K^{-1}). The plots of log CR against 1 / 2.303 RT exhibit straight lines with a slope corresponding to E_a and intercept to log A.

Enthalpy (ΔH^*/ kJ mol^{-1}) and entropy (ΔS^* / J mol^{-1} K^{-1}) of activation were obtained from the slope -ΔH^*/2.303R and intercept [log R/Nh + (ΔS^* / 2.303 R)] respectively from the plot of log (CR/T) versus 1 / T in accordance with the following alternative form of Arrhenius Equation (5):

$$\log\frac{\mathrm{CR}}{T} = \frac{-\Delta H^*}{2.303R}\left(\frac{1}{\mathrm{T}}\right) + \left[\log\frac{R}{N_A h} + \left(\frac{\Delta S^*}{2.303R}\right)\right] \quad (5)$$

where h signifies Planck's constant, N_A denotes Avogadro's number, T represents thermodynamic temperature, R denotes the universal gas constant, ΔS^* is the entropy change, and ΔH^* signifies the enthalpy change.

Adsorption and thermodynamics

In corrosion science, adsorption isotherms describe the adsorption behavior of corrosion inhibitors on metal surfaces. They help to determine the thermodynamic parameters and the nature of the interaction of inhibitors with the metal surface (physisorption or chemisorption), as well as estimate the efficiency of these interactions. For this purpose, the adsorption models of Langmuir, Temkin, Freundlich, Flory-Huggins, Frumkin and El-Awady (Equations (6) to (11)) are usually used. Every model has its own mathematical form, allowing graphical determination of the necessary parameters [22]. In our study, we evaluated the applicability of all the above models to the adsorption of AQ2SNa on the surface of carbon steel in accordance with their mathematical expressions, where C_{inh} / g dm^{-3} - inhibitor concentration, θ - degree of surface coverage, K_{ads} - the equilibrium constant for adsorption-desorption processes:

- Langmuir adsorption isotherm

$$\frac{C_{inh}}{\theta} = \frac{1}{K_{ads}} + C_{inh} \quad (6)$$

- Temkin adsorption isotherm

$$\theta = \ln C_{inh} + K_{ads} \quad (7)$$

- Freundlich adsorption isotherm

$$\log\theta = \log K_{ads} + \frac{1}{n}\log C_{inh} \quad (8)$$

where n is a dimensionless constant indicating the intensity of the adsorption process.

- Flory-Huggins adsorption isotherm

$$\log\frac{\theta}{C_{inh}} = b\log(1-\theta) + \log K_{ads} \quad (9)$$

where b is the parameter representing the interaction between the adsorbate and the adsorbent.

- Frumkin adsorption isotherm

$$\log\left[C_{inh}\left(\frac{\theta}{1-\theta}\right)\right] = 2\alpha\theta + 2.303\log K_{ads} \quad (10)$$

where α is the interaction parameter that quantifies the interactions between adsorbed molecules on the surface.

- El-Awady adsorption isotherm

$$\log\left(\frac{\theta}{1-\theta}\right) = y\log C_{\text{inh}} + \log K \qquad K_{\text{ads}} = K^{\frac{1}{y}} \tag{11}$$

where y is the parameter that represents the number of active sites occupied by one inhibitor molecule on the metal surface.

The values of K_{ads} obtained from the isotherms are usually used to calculate the Gibbs free energy according to the known relationship:

$$\Delta G^0_{ads} = -RT\ln(55.5\,K_{\text{ads}}) \tag{12}$$

where ΔG^0_{ads} is the Gibbs free energy of adsorption, R is the universal gas constant, T is the thermodynamic temperature, and 55.5 is the molar concentration of water in mol dm^{-3}.

Electrochemical measurements

The steel specimens used in the electrochemical experiment and weight loss tests underwent the same pretreatment. The NOVA 2.1.6 software installed in the Autolab PGSTAT 101 Metrohm potentiostat/galvanostat was used for the electrochemical test. Electrochemical measurements were conducted using a three-electrode configuration: a reference electrode (Ag/AgCl filled with 3.0 mol dm^{-3} KCl), a counter electrode (platinum), and a working electrode (steel sample). An electrochemical cell was created using a beaker with 100 ml of 0.5 mol dm^{-3} H_2SO_4, with and without inhibitor. During open circuit potential (OCP) testing, the working electrode, with an exposed area of 1.0 cm^2, was stabilized. Linear polarization measurements were carried out immediately following the OCP using linear sweep voltammetry (LSV) staircase and corrosion rate analysis. Potentiodynamic scanning was conducted by applying a scan rate of 0.01 V s^{-1} within the range of -0.50 to +0.50 V. The corrosion potential (E_{corr}) and corrosion current density (j_{corr}) were determined from Tafel polarization curves.

Equation (13) was utilized to calculate the inhibition efficiency (IE$_j$, %) based on the corrosion current density:

$$\text{IE}_j = \frac{j_{\text{inh}} - j_{\text{corr}}}{j_{\text{inh}}}100 \tag{13}$$

where j_{inh} and j_{corr} are the corrosion current densities determined by extrapolating the Tafel slopes with and without inhibitors, respectively, A cm^{-2}.

The calculation of inhibition efficiency through polarization resistance (IE$_R$, %) was derived using the Equation (14):

$$\text{IE}_R = \frac{\text{R}_\text{p}^{\text{inh}} - \text{R}_\text{p}^{0}}{R_\text{p}^{\text{inh}}}100 \tag{14}$$

where R_p^{inh} and R_p^0 / Ω represent the charge transfer resistance with and without inhibitor, respectively.

Metal surface analysis

Contact angle measurement

The hydrophilicity of the steel coupons was assessed by measuring the contact angle between a water drop and the steel surface using an Ossila Contact Angle Goniometer equipped with the Ossila Contact Angle software *ver.* 4.2.0. The water drops were mounted on the surface of the carbon steel sample using a micro-syringe with a needle diameter of 0.4 mm. The reported contact angles were an average of at least three measurements from different areas of the surface. Photos of water drops were obtained using a high-resolution video camera and the above software.

Scanning electron microscopy surface analysis

Scanning electron microscopy (SEM) accurately reflect the morphology of the metal surface after corrosion and provides a very valuable reference for evaluating corrosion inhibitor performance. A scanning electron microscope JEOL 6390LV was used to observe the surface morphologies of the carbon steel specimens after immersion in 0.5 mol dm^{-3} H_2SO_4 solution with and without inhibitor for 24 h. Tested specimens were compared with the polished specimens to analyze the corrosion inhibition efficiency. Before the experiments, the carbon steel surface was thoroughly cleaned with ethanol and acetone. Then, the polished specimen and the specimens after immersion in 0.5 mol dm^{-3} H_2SO_4 solution were examined in the absence or presence of AQ2SNa for 24 h.

Computational details

Computer modeling methods such as density functional theory (DFT) calculation and molecular dynamic (MD) simulation are required for the theoretical study of new corrosion inhibitors. For this purpose, both methods were used in this work.

Quantum chemical calculations

The molecular mechanism of corrosion inhibition can be well explained by quantum chemical calculations. It is a valuable tool for gaining deeper insight into the adsorption phenomena and the accompanying effects of electronics.

In an aggressive environment, corrosion inhibitors can undergo various chemical transformations [23]. In acidic environments, AQ2SNa can dissociate as an ionic compound *via* Equation (15) or form the corresponding acid according to the exchange reaction described by Equation (16). Acid formed can also dissociate in solution and produce ions described by Equation (17):

$$AQ2SNa \leftrightarrows AQ2S^- + Na^+ \quad (15)$$

$$AQ2SNa + H^+ \leftrightarrows AQ2SH + Na^+ \quad (16)$$

$$AQ2SH \leftrightarrows AQ2S^- + Na^+ \quad (17)$$

According to Equations (15) to (17), in a solution, AQ2SNa can exist as a salt, an acid (AQ2SH), and sulfonate ions ($AQ2S^-$). Therefore, quantum chemical calculations were carried out for the three indicated forms for a comparative assessment. The energy of the highest occupied molecular orbital (E_{HOMO}), the energy of the lowest unoccupied molecular orbital (E_{LUMO}), energy gap (ΔE_{gap}), the ionization potential (IP), the electron affinity (EA), electronegativity (χ), global hardness (η), softness (σ), electrophilic (ω) and nucleophilic (ε) indexes, back-donation energy ($E_{b\text{-}d}$), total negative charge (TNC, TNC/n) were considered (n - total number of atoms in molecule) [24].

All quantum chemical calculations were performed on a desktop PC with Windows 11, a 12^{th} generation Intel(R) Core (TM) i7-12700H 2.30 GHz, 16GB RAM) with GAMESS software [25]. Initially, full geometry optimization was achieved using the Molecular Mechanics (MM+) force field. The results from MM+ were further selected as input and re-optimized using semi-empirical AM1 to obtain the equilibrium geometry. Final geometry optimization and quantum chemical parameters were obtained by density functional theory (DFT) calculations. DFT is the most widely accepted *ab initio* approach for modeling ground states of molecules. To calculate optimized geometrical structure, atomic charges, and energies, the Lee-Yang-Parr Becke's three-parameter hybrid functionnal method (B3LYP) with the split-valence double-zeta polarized basis set 6-311+G(d,p) was used. All DFT calculations were done in the aqueous phase because it is well-known that the electrochemical corrosion always appears in an aqueous medium. The solvent (H_2O) was incorporated via the Conductor-like Screening Model (COSMO) [26].

Molecular dynamics simulation

The intensity of the interactions between the examined inhibitor and metal surface was determined using molecular dynamics (MD) simulations. MD simulation is a modern computational technique crucial for theoretical studies of the interaction between inhibitors and metal surfaces.

The corrosion system, which is composed of carbon steel, water, and a corrosion inhibitor structure, was constructed using Avogadro software. The MD simulations were carried out by using the GROMACS 2020.4 software [27]. Adsorption energy was calculated by Equation (18):

$$E_{adsorption} = E_{total} - (E_{Fe(110)+solution} + E_{inhibitor}) \quad (18)$$

where $E_{adsorption}$ is the adsorption energy (or interaction energy) corresponds to the amount of energy released or absorbed as 1 mole of adsorbate molecules is adsorbed on the adsorbent, E_{total} is the total energy of the whole system (surface Fe(110) + solution + inhibitor molecule), $E_{Fe(110)+solution}$ is the energy of the metal and the aqueous phase and $E_{inhibitor}$ is the energy of the inhibitor molecule.

Binding energy is the energy required to separate a particle from a system. The greater the binding energy, the stronger the attraction force between the inhibitor and the metal surface, and hence the higher the inhibition efficiency. The binding energy is regarded as the reciprocal of the adsorption energy of the inhibitor molecule as follows (19):

$$E_{binding} = -E_{adsorption} \quad (19)$$

where $E_{binding}$ is the binding energy.

Five layers of Fe (110) metal containing 960 Fe atoms were placed at the bottom of a simulation box, with the corrosion inhibitor molecule placed at the center of the box, surrounded by 800 water molecules (periodic boundary conditions). The Fe (110) metal structure was chosen due to its lowest surface energy, thermodynamic stability and the largest area of the Fe crystal [28]. Before the MD simulation, the system was optimized until the energy met the 0.10 J mol value. MD was conducted at a constant temperature of 298 K, with a 1 fs time step and a simulation time of 500 ps.

Results and discussion

Weight loss analysis

The weight loss tests were performed using the inhibitor concentrations of 0.05, 0.1, 0.2, 0.3, 0.4, and 0.5 g dm^{-3} for an exposure period of 2-24 hours. Figure 2 illustrates the impact of AQ2SNa concentration and exposure duration on the *CR* (A) and IE (B) of carbon steel in 0.5 mol dm^{-3} H_2SO_4 solutions.

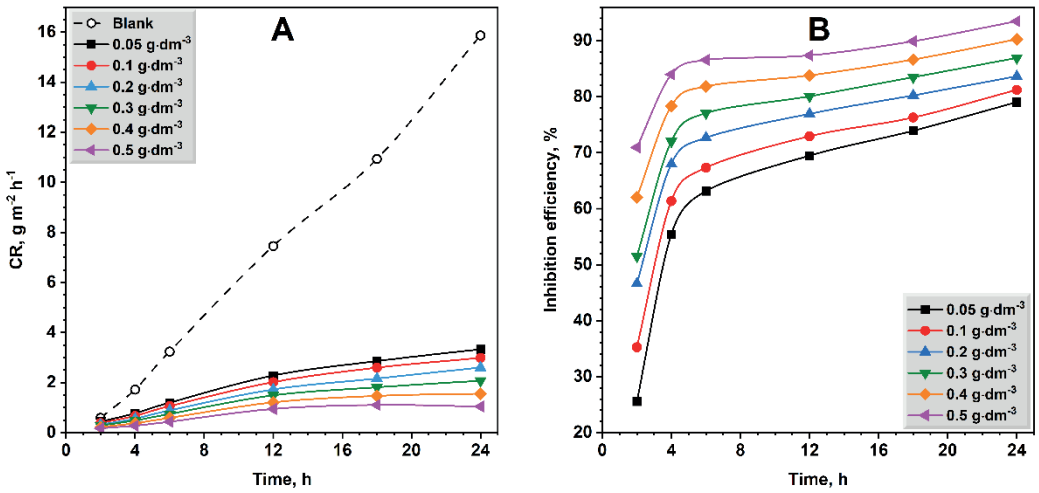

***Figure 2**. The relationship between CR (A) and IE (B) on carbon steel in 0.5 mol dm^{-3} H_2SO_4 solution and immersion time and inhibitor concentration at room temperature*

Evidently, the presence of AQ2SNa significantly decreases the corrosion rate (Figure 2A). The IE of AQ2SNa in 0.5 mol dm^{-3} H_2SO_4 depends on the inhibitor concentration and increases with the exposure time. The existence of an induction period indicates that the inhibitor forms the most effective protective layer on the carbon steel surface after at least 4 to 6 hours of immersion. The increase in the inhibitor concentration results in the augmentation of the protective properties. It was found that an inhibitor concentration of 0.5 g dm^3 provided the most effective corrosion inhibition. Accordingly, for the best possible inhibition, the inhibitor should be used in higher concentrations. The obtained results suggest that AQ2SNa has promising applications for preventing metal corrosion in a strongly acidic environment.

The corrosion rate (CR), inhibition efficiency (IE), and degree of surface coverage (θ) obtained from weight loss assay for carbon steel in 0.5 mol dm^{-3} H_2SO_4 solution at 298, 303, 313, 323 and 333 K in the absence and presence of AQ2SNa are given in Table 1.

Table 1. *Corrosion parameters obtained from weight loss assay of carbon steel in 0.5 mol dm^{-3} H_2SO_4 containing various concentrations of AQ2SNa at different temperatures*

Inhibitor concentration / g dm^{-3}	CR / g m^{-2} h^{-1}	IE / %	θ
	298 K		
0.00	6.30 ± 0.28	-	-
0.05	2.03 ± 0.12	67.81 ± 2.01	0.6781
0.10	1.89 ± 0.10	70.05 ± 1.25	0.7005
0.20	1.70 ± 0.08	73.04 ± 1.92	0.7304
0.30	1.38 ± 0.06	78.04 ± 1.79	0.7804
0.40	1.22 ± 0.05	80.66 ± 1.65	0.8066
0.50	1.01 ± 0.03	84.02 ± 1.85	0.8402
	303 K		
0.00	13.47 ± 0.84	-	-
0.05	3.78 ± 0.25	71.92 ± 2.38	0.7192
0.10	3.45 ± 0.19	74.38 ± 2.05	0.7438
0.20	3.09 ± 0.16	77.05 ± 1.99	0.7705
0.30	2.46 ± 0.13	81.72 ± 2.16	0.8172
0.40	2.12 ± 0.13	84.29 ± 2.48	0.8429
0.50	1.69 ± 0.10	87.49 ± 2.59	0.8749
	313 K		
0.00	27.97 ± 1.87	-	-
0.05	7.50 ± 0.82	73.19 ± 2.03	0.7319
0.10	6.64 ± 0.68	76.27 ± 2.60	0.7627
0.20	5.39 ± 0.52	80.74 ± 2.59	0.8074
0.30	4.31 ± 0.33	84.58 ± 2.75	0.8458
0.40	3.26 ± 0.27	88.36 ± 3.16	0.8836
0.50	2.18 ± 0.16	92.22 ± 3.38	0.9222
	323 K		
0.00	47.93 ± 3.24	-	-
0.05	9.72 ± 0.56	79.72 ± 2.29	0.7972
0.10	8.50 ± 0.32	82.26 ± 3.09	0.8226
0.20	7.18 ± 0.29	85.02 ± 2.94	0.8502
0.30	5.66 ± 0.28	88.20 ± 3.36	0.8820
0.40	4.39 ± 0.21	90.85 ± 3.24	0.9085
0.50	3.03 ± 0.16	93.67 ± 3.04	0.9367
	333 K		
0.00	65.06 ± 3.84	-	-
0.05	12.45 ± 1.03	80.86 ± 2.23	0.8086
0.10	10.88 ± 0.86	83.28 ± 2.81	0.8328
0.20	9.02 ± 0.72	86.13 ± 3.12	0.8613
0.30	7.12 ± 0.56	89.06 ± 3.27	0.8906
0.40	5.40 ± 0.47	91.69 ± 2.93	0.9169
0.50	3.62 ± 0.34	94.44 ± 3.11	0.9444

Table 1 shows that the best protective efficiency of 94.44 % is achieved at the highest temperature and concentration values. The obtained values of corrosion rates and protective effect clearly indicate an enhancement in the inhibitory effectiveness of AQ2SNa with the increased temperature and concentration in a given corrosion medium. At all temperatures, the IE reaches its maximum value at the highest concentration of the inhibitor. The results show that the presence of AQ2SNa decreases metal dissolution in 0.5 mol dm^{-3} H_2SO_4 medium. This effect can be interpreted because of the formation of the protective layer of the inhibitor on the carbon steel surface.

Activation parameters

Graphical representation of activation parameters determined from the Arrhenius plots and transition state plots in accordance with Eqs. (4) and (5) are presented in Figure 3.

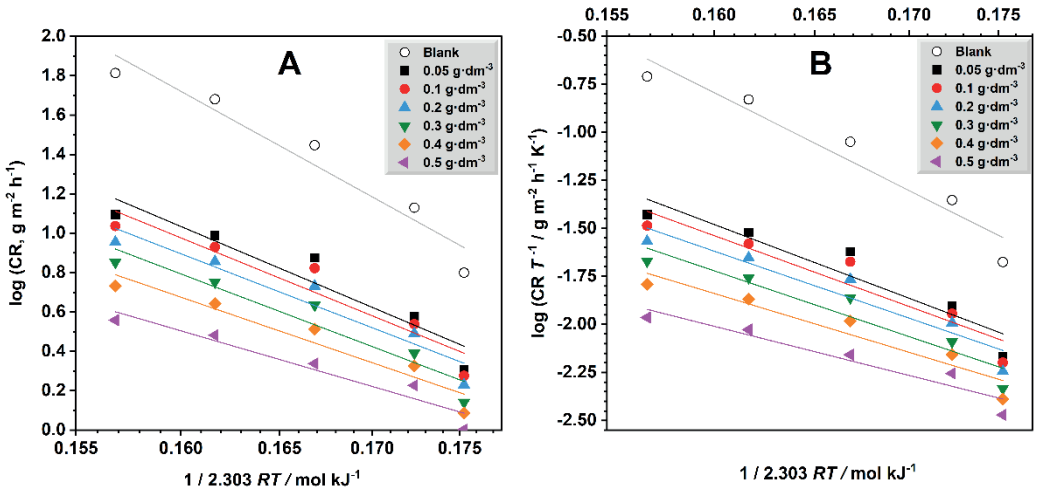

***Figure 3**. Arrhenius plots (A) and transition state plots (B) for carbon steel in 0.5 mol dm^{-3} H_2SO_4 solution in the absence and presence of AQ2SNa at different concentrations*

The activation parameters of corrosion of carbon steel in 0.5 mol dm^{-3} H_2SO_4 in the absence and presence of different concentrations of AQ2SNa are given in Table 2.

***Table 2**. Activation parameters of the dissolution of carbon steel in 0.5 mol dm^{-3} H_2SO_4 in the absence and presence of different concentrations of AQ2SNa*

Inhibitor concentration / g dm^{-3}	A	E_a / kJ mol^{-1}	ΔH^* / kJ mol^{-1}	ΔS^* / J mol^{-1} K^{-1}
Blank	$2.52 \cdot 10^7$	27.95	-26.57	-378.80
0.05	$8.98 \cdot 10^5$	21.41	-20.03	-351.07
0.1	$5.66 \cdot 10^5$	20.62	-19.24	-347.24
0.2	$3.11 \cdot 10^5$	19.57	-18.19	-342.27
0.3	$3.05 \cdot 10^5$	19.23	-17.85	-342.10
0.4	$9.73 \cdot 10^4$	17.35	-15.97	-332.59
0.5	$2.00 \cdot 10^4$	14.72	-13.34	-319.44

In the presence of AQ2SNa, the activation energy is lower than that in the uninhibited sulfuric acid solution, which means that the inhibitor is effectively reducing the energy required for the corrosion reaction to proceed, thereby slowing down the corrosion rate. The decrease of activation energy with an increase in the inhibitor concentration leads to better surface coverage and more effective corrosion inhibition [29].

A decrease in the pre-exponential factor (A) with an increase in inhibitor concentration suggests a reduction in the frequency of effective molecular collisions, which can be attributed to various factors that hinder molecular interactions. In corrosion studies, this indicates that the inhibitor is effectively adsorbing onto the surface, forming a barrier that reduces the number of active sites available for the

reaction [30]. The negative values of the enthalpy of activation (ΔH^*) indicate that the process is exothermic, suggesting that the reaction is energetically favorable and tends to proceed spontaneously at lower temperatures [31]. An increase in ΔH^* with temperature suggests that at higher temperatures, the system needs more energy to sustain the reaction, and the energy barrier for the corrosion process becomes higher as the temperature rises. This behavior is often observed in systems where the inhibitor's effectiveness improves with temperature, leading to a more stable and protective adsorbed layer on the metal surface [32]. The negative values of the entropy of activation (ΔS^*) indicate that the transition state of the corrosion process is more ordered than the initial state. This implies that the formation of the activated complex involves a decrease in randomness or an increase in order. It also indicates that the activated complex is formed through an association process rather than dissociation, and the inhibitor molecules combine in a more ordered manner to form the transition state. The increase of the ΔS^* indicates that the rise in temperature corresponds to additional freedom of movement acquired by inhibitor molecules, leading to a less ordered transition state. This phenomenon often accompanies an endothermic process, where the adsorption and activation processes become more favorable at higher temperatures.

Adsorption and thermodynamics

Adsorption isotherms for AQ2SNa on carbon steel in 0.5 mol dm^{-3} H_2SO_4 surface, calculated according to Equations (6) to (11) at all experimental temperatures, are given in Figure 4. Figure 4A shows that $C\,\theta^{-1}$ presented *versus* inhibitor concentration at all experimental temperatures exhibits the best straight lines. High values of the linear regression coefficient ($r^2 > 0.995$) indicate that the Langmuir isotherm is the most suitable for describing the adsorption of AQ2SNa on the surface of carbon steel. The agreement of the adsorption process with the Langmuir model indicates that the inhibitor molecules form a monolayer on the metal surface, displacing the water molecules that initially occupy the adsorption sites, and no further adsorption occurs when the surface is completely covered [33]. It also demonstrates that all adsorption sites on the metal surface are identical and energetically equivalent and the adsorbed molecules do not interact with each other, meaning that the adsorption of one molecule does not affect the adsorption of another molecule [34]. For other isotherms, the value of the linear regression coefficient is significantly lower, rendering them unfit for describing the process of adsorption of AQ2SNa on a carbon steel surface under given experimental conditions.

The K_{ads} and Gibbs free energy values (ΔG^0_{ads}) for the AQ2SNa were calculated from the slopes and intercepts of the Langmuir adsorption isotherms in Figure 4A and presented in Table 3.

Table 3. *Thermodynamic parameters of adsorption of AQ2SNa on carbon steel surface in 0.5 mol dm^{-3} H_2SO_4 solution*

T / K	Slope	Intercept	r^2	K_{ads} / 10^{-3} dm^3 g^{-1}	ΔG^0_{ads} / kJ mol^{-1}
298	1.15823	0.02841	0.99709	35.20	-18.78
303	1.11599	0.02449	0.99760	40.83	-19.47
313	1.05535	0.02232	0.99695	44.80	-20.35
323	1.04882	0.01851	0.99848	54.02	-21.50
333	1.04118	0.01714	0.99824	58.34	-22.38

Negative values of ΔG^0_{ads} indicate that the absorption of AQ2SNa onto the carbon steel surface is spontaneous. The value of $\Delta G^0_{ads} > -20$ kJ mol^{-1} clearly shows that the adsorption is physical (physi-sorption) and occurs as a result of electrostatic interaction between charged inhibitor molecules and the steel surface.

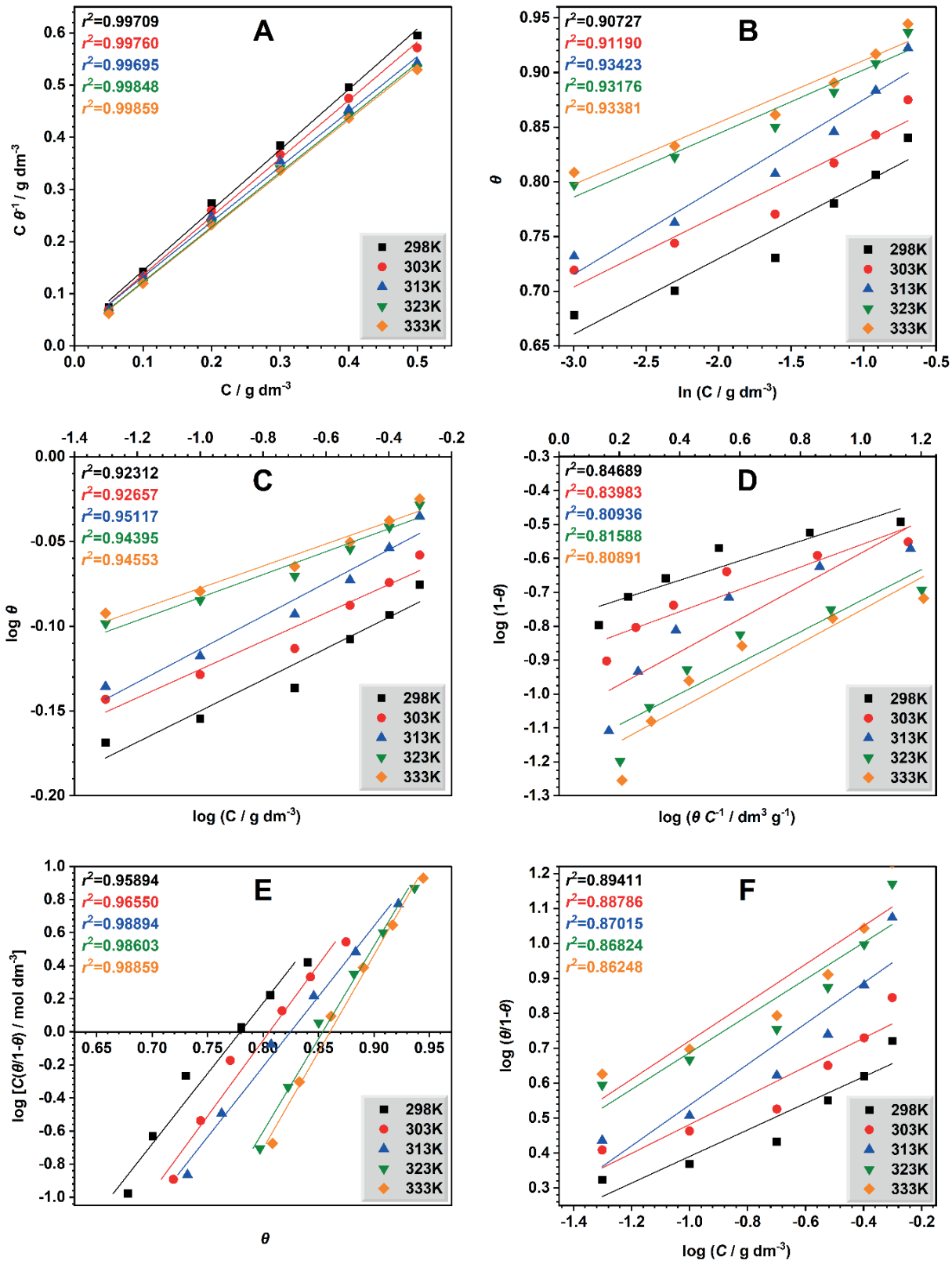

***Figure 4**. Adsorption isotherms for AQ2SNa in 0.5 mol dm^{-3} H_2SO_4 for 4 hours immersion period: A - Langmuir, B - Temkin, C - Freundlich, D - Flory-Huggins, E - Frumkin, F - El-Awady (r^2 - linear regression coefficient)*

Increasing the temperature and concentration of the inhibitor accelerates the adsorption-desorption processes and promotes the formation of a stable, protective barrier on the metal surface [35]. A decrease in the Gibbs free energy value indicates that with an increase in temperature, adsorption occurs more efficiently, which contributes to better corrosion protection.

The values of ΔH^0_{ads} and ΔS^0_{ads} were calculated from the obtained values of ΔG^0_{ads} using the rearranged Gibbs-Helmholtz Equation (20):

$$\Delta G^0_{ads} = \Delta H^0_{ads} - T\Delta S^0_{ads} \quad (20)$$

The slope and intercept of the plot of the relationship between ΔG^0_{ads} and T allow to determine the values of ΔS^0_{ads} and ΔH^0_{ads}, respectively (Figure 5).

The positive value of ΔH^0_{ads} (11.62 kJ mol^{-1}) reveals that the adsorption of inhibitor molecules is an endothermic process and suggests physical adsorption (physisorption). It also indicates that the adsorption process becomes more favorable at higher temperatures, as the increased thermal energy helps to overcome the activation barrier for the adsorption reaction [36].

A positive value of ΔS^0_{ads} (102.28 J mol^{-1} K^{-1}) for AQ2SNa indicates an increase in disorder at the metal-solution interface during the adsorption of inhibitor molecules onto the metal surface. Such values of ΔS^0_{ads} are often associated with endothermic adsorption (positive ΔH^0). Since the adsorption of inhibitor molecules onto the metal surface in aqueous corrosion media occurs with the displacement of water molecules, their subsequent desorption into the solution increases the overall disorder, thus contributing to a positive ΔS^0 value.

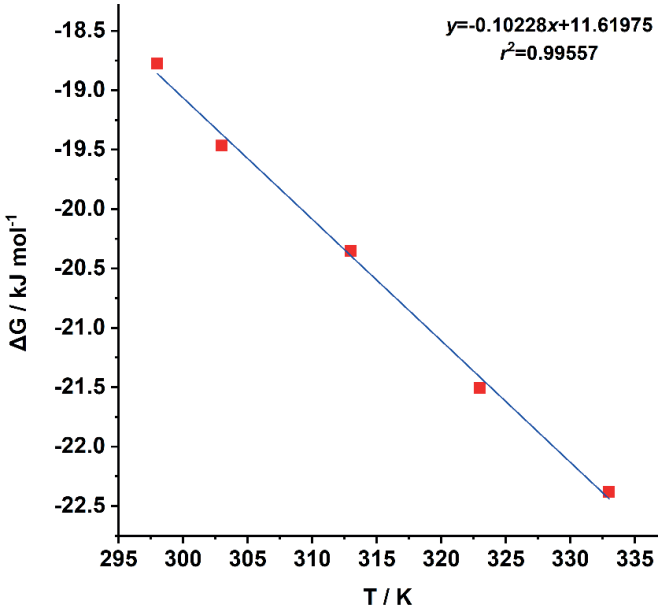

Figure 5*. The relationship between Gibbs free energy (ΔG^0_{ads}) and absolute temperature for adsorption of AQ2SNa on carbon steel in 0.5 mol dm^{-3} H_2SO_4 solution*

Metal surface analysis

Contact angle measurement was carried out to verify the formation of a protective layer of AQ2SNa inhibitor molecules on the carbon steel surface by evaluating changes in surface properties. This experiment provides insights into the surface wettability and the effectiveness of the inhibitor. A higher contact angle indicates increased hydrophobicity, suggesting that the inhibitor forms a protective layer on the metal surface, reducing its wettability and potentially enhancing corrosion resistance. Figure 6 displays the values of the contact angles for the carbon steel surface both with and without the inhibitor, taken before and after immersion in a 0.5 mol dm^{-3} H_2SO_4 solution.

Figure 6 shows that the contact angle on the clean carbon steel surface is 55.96±0.82° before immersion in a corrosive environment. After 24 hours of exposition in 0.5 mol dm^{-3} H_2SO_4 without the addition of an inhibitor, the contact angle was determined as 64.17±0.73°.

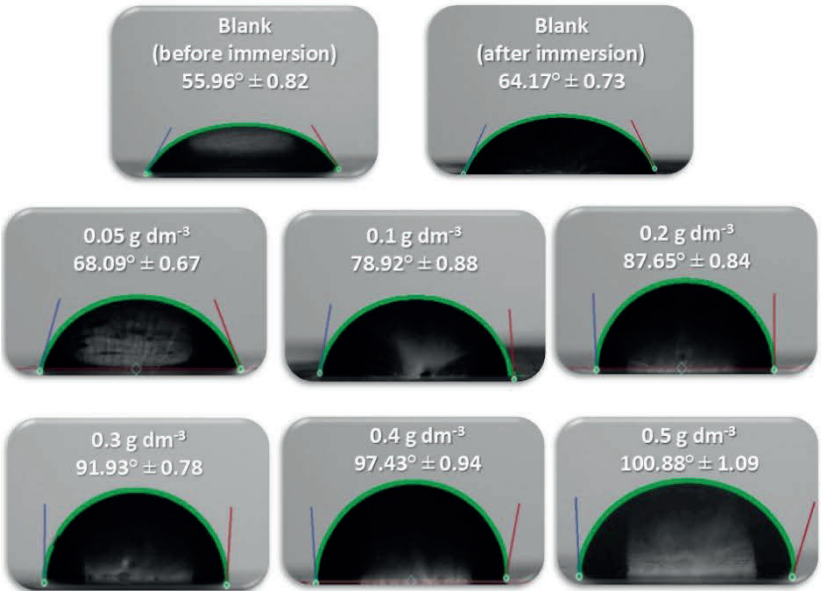

Figure 6. *Contact angle values before and after immersing the carbon steel in 0.5 mol dm^{-3} H_2SO_4 solution for 24 hours in the presence of different AQ2SNa inhibitor concentrations*

In the presence of an inhibitor, the contact angle increases significantly depending on the inhibitor concentration and reaches 100.88±1.09° at the maximal AQ2SNa concentration after 24 hours of immersion. The increase in the contact angle with increasing inhibitor concentration indicates increased hydrophobicity of the carbon steel surface. This suggests that the inhibitor effectively adsorbs on the surface, forming a protective layer that reduces wettability. As the inhibitor concentration increases, this layer becomes more robust, preventing the corrosive solution from interacting with the metal surface.

Scanning electron microscopy surface analysis

In order to explore the inhibitory properties of AQ2SNa better, the surface morphology of carbon steel was analyzed. Figure 7 shows the SEM micrographs of the polished steel and carbon steel immersed in 0.5 mol dm^{-3} H_2SO_4 solution at 298 K for 24 h in the absence and presence of 0.5 g dm^{-3} AQ2SNa.

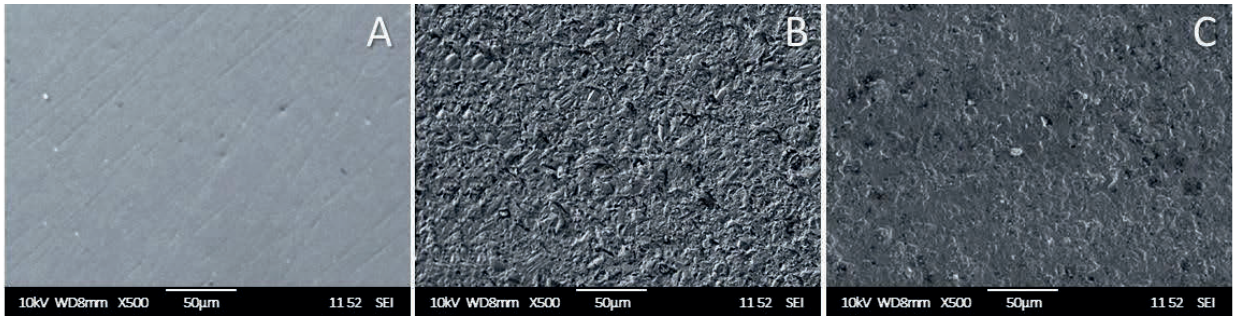

Figure 7. *SEM micrographs of mild steel polished (A), after immersion without (B) and with (C) 0.5 g dm^{-3} AQ2SNa in 0.5 mol dm^{-3} H_2SO_4 solution*

As can be seen, before immersion into the corrosion medium, the surface of the polished carbon steel was smooth, homogeneous with metallic lustre and a clearly defined structure, and the entire surface had some negligible roughness and scratches which are caused by sanding the prepared specimen (Figure 7A). After an immersion period without inhibitor, a drastic change in the metal surface structure is observed, forming a uniform dark, friable layer with noticeable pits and cracks. It can be observed that without the inhibitor, the carbon steel surface was severely corroded and

oxidized and corrosion pits appeared (Figure 7B). Compared with the fresh steel, the specimen surface was seriously damaged due to the corrosive acid solution in the absence of the inhibitor. This indicated carbon steel was corroded in 0.5 mol dm^{-3} H_2SO_4 solution. The presence of AQ2SNa induces the formation of a protective layer and the disappearance of the metallic lustre; however, the structure of the metal surface remains almost completely intact and visible corrosion damage to the surface is significantly reduced, which indicates that AQ2SNa exhibits excellent corrosion inhibition on carbon steel surface (Figure 7C). When the inhibitor was added to the corrosion medium, the carbon steel surface became smoother and cleaner because a protective film formed. These observations indicated that the inhibitor molecules adsorbed on the surface of carbon steel to form a protective film, which prevents the corrosion resulting from the corrosive medium.

Electrochemical experiments

Figure 8 displays the OCP *vs*. time curves and Tafel polarization curves for carbon steel corrosion in 0.5 mol dm^{-3} H_2SO_4. The OCP evaluation was performed during 60 seconds of immersion, both with and without AQ2SNa.

Figure 8 clearly demonstrates the anodic and cathodic polarization responses of carbon steel coupons, while Table 4 enlists the related corrosion outcomes and inhibition efficiencies obtained from polarization curves through corrosion rate analysis. The OCP reached an equilibrium state prior to the 60-second expiry. A shift in the OCP value at various AQ2SNa concentrations indicates that inhibitor molecules have adsorbed to the surface of the carbon steel. As can be seen, AQ2SNa primarily inhibits the anodic process, as indicated by a positive shift in OCP.

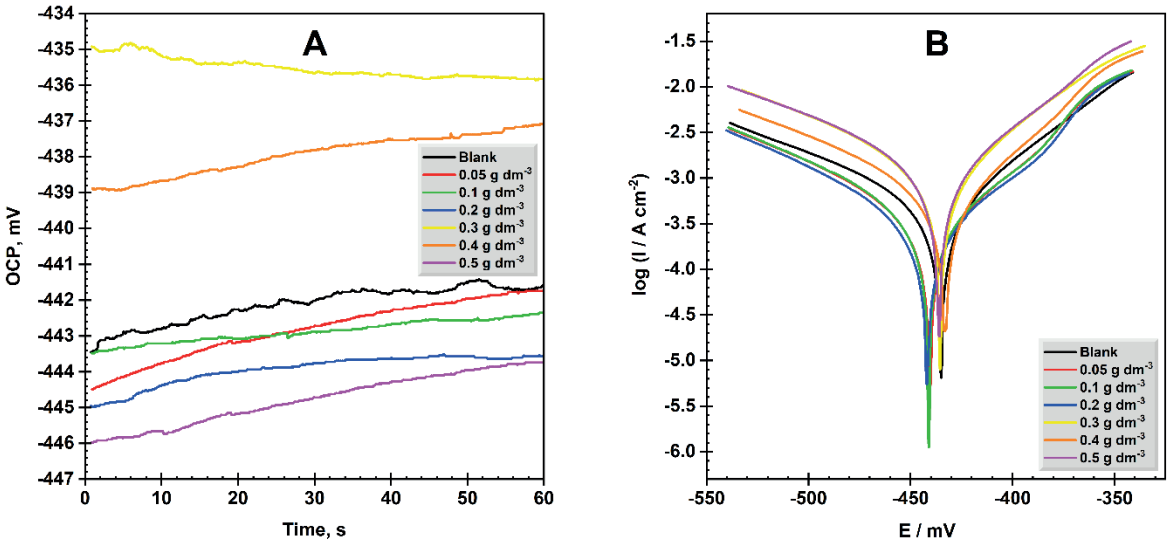

***Figure 8**. OCP vs. time diagram (A) and Tafel polarization curves (B) for carbon steel in 0.5 mol dm^{-3} H_2SO_4 solution with and without AQ2SNa at room temperature*

***Table 4**. The electrochemical parameters of carbon steel corrosion in 0.5 mol dm^{-3} H_2SO_4 in the absence and presence of different concentrations of aqueous solution of AQ2SNa at room temperature*

Inhibitor concentration / g dm^{-3}	$-E_{corr}$ / mV	j_{corr} / 10 nA cm^{-2}	IE_j / %	$\lvert b_a \rvert$ / mV dec^{-1}	$\lvert b_c \rvert$ / mV dec^{-1}	R_p / Ω	IE_R / %
Blank	432.98 ± 9.28	315 ± 9.5	-	71.13	91.09	60.37 ± 2.96	-
0.05	435.08 ± 8.36	87.2 ± 1.9	72.39	76.75	113.58	300.51 ± 12.33	79.91
0.1	440.46 ± 7.09	82.4 ± 2.2	73.88	88.68	121.26	354.85 ± 14.81	82.99
0.2	436.05 ± 6.53	74.5 ± 1.7	76.39	81.21	113.49	362.94 ± 16.86	83.37
0.3	435.08 ± 7.15	67.7 ± 2.1	78.55	75.13	105.56	370.34 ± 19.21	83.70
0.4	433.96 ± 6.13	61.1 ± 1.2	80.65	81.14	110.07	436.91 ± 22.78	86.18
0.5	432.98 ± 8.41	56.1 ± 1.5	82.23	84.05	113.14	451.91 ± 23.57	86.64

The corrosion rate of carbon steel in 0.5 mol dm^{-3} H_2SO_4 is significantly reduced in the presence of AQ2SNa. The presence of the inhibitor leads to significantly lower corrosion current density (J_{corr}) values, indicating that the metal surface is sufficiently protected from corrosion by AQ2SNa. The addition of an inhibitor leads to an increase in the values of polarization resistance (R_p), which confirms the formation of a protective layer on the steel surface, thereby preventing corrosion damage [37]. Apparently, the presence of an inhibitor causes a discernible shift in both the cathodic and anodic sites of the polarization curves, due to which AQ2SNa slows down both the cathodic and anodic reactions and acts as a mixed-type inhibitor. The anodic $|b_a|$ shift is smaller than the cathodic site shifts $|b_c|$, indicating the greater effect of the inhibitor on cathodic polarization rather than anodic polarization.

The values of the inhibitory effect, ascertained by applying Equations (13) and (14) based on corrosion current and polarization resistance, respectively, in the presence of the AQ2SNa aqueous solution, rise noticeably as the concentration of the inhibitor increases. This suggests that the investigated inhibitor has a high potential to stop the corrosion of carbon steel in a solution of 0.5 mol dm^{-3} H_2SO_4.

Quantum chemical calculations

Top and side views of the optimized structures calculated using DFT/B3LYP/6-311+G(d,p) of AQ2SNa, AQ2SH, and $AQ2S^-$ are shown in Figure 9.

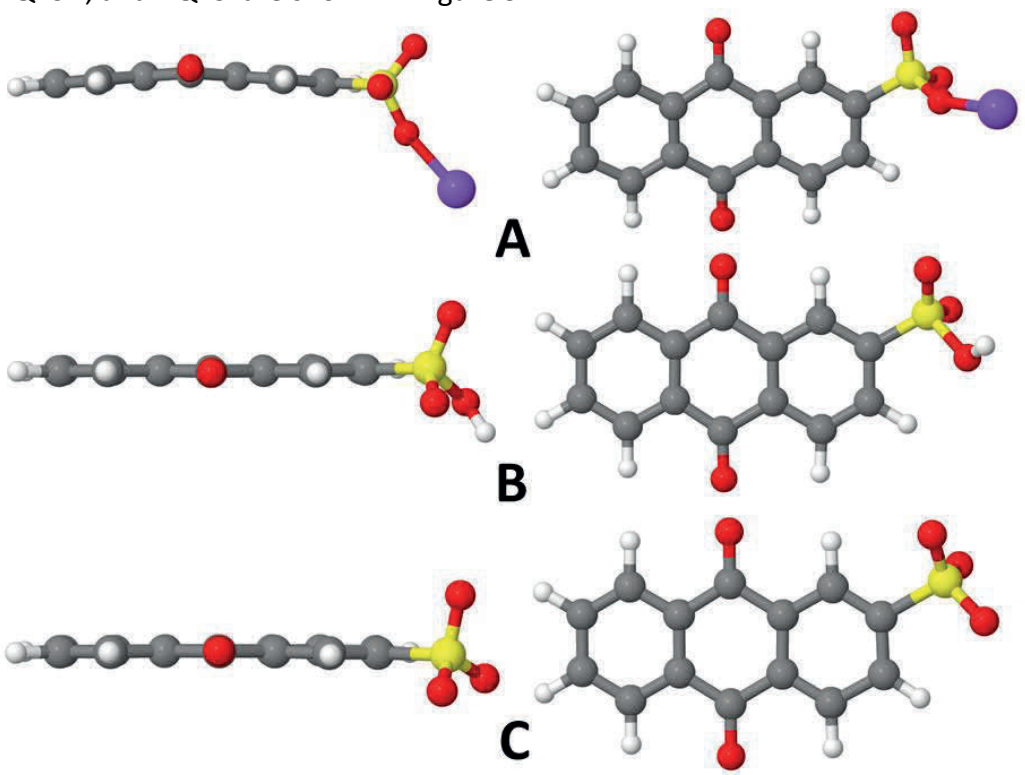

Figure 9. *Top and side view of the optimized structures of AQ2SNa (A), AQ2SH (B) and $AQ2S^-$ (C) calculated using DFT/B3LYP/6-311+G(d,p)*

As can be seen, the acidic and ionic forms of the inhibitor molecule are flat structures. Nevertheless, the sodium salt molecule is slightly bent in the middle at an angle of 172.1° and is not an absolutely flat structure. This indicates that the sorption of the inhibitor molecule in the form of a sodium salt could be relatively hindered.

Mulliken charges distribution

The distribution of electron density has a major impact on a molecule's chemical reactivity. The electrophilic and nucleophilic centers of the molecule can be identified through the use of Mulliken atomic charge distribution (MACD) analysis, which is a valuable parameter for the designation of the accountable atoms of the corrosion inhibitors that are prone to adsorption onto the metals. The carbon steel surface and the inhibitor molecules interact on the atoms with a large negative charge. The MACD with corresponding values of total negative charge (TNC) and TNC/n for different forms of the inhibitor molecule are shown in Table 5.

The MACD values in Table 5 indicate that the largest negative charges are in the ionic form ($AQ2S^-$) of inhibitor molecule and located on oxygen atoms, indicating that these centers have the highest electron density and interact with Fe (110). This electron density is also visible in Figure 10 in the visualized molecular electrostatic potential (MEP) for inhibitor molecules.

TNC refers to the sum of the negative charges on all atoms within a molecule. Molecules with higher TNC tend to have a greater ability to donate electrons to the metal surface. A higher TNC indicates stronger interactions between the inhibitors and the metal surface. This is because the negatively charged regions of the molecule can interact more effectively with the positively charged metal atoms, enhancing the stability of the adsorbed layer [38].

The most negative values of TNC and TNC/*n* were calculated for the ionic form of the inhibitor molecule (-3.6542 and -0.1305, respectively). This indicates a greater tendency of the ionic form of the inhibitor to adsorb on the metal surface and, consequently, to exhibit inhibitory properties.

Table 5. *Mulliken atomic charge distribution, TNC and TNC/n for different forms of AQ2SNa (atomic enumeration corresponds to Figure 1)*

	Atom	AQ2SNa	AQ2SH	$AQ2S^-$
MACD	C(1)	-0.0912	-0.0806	-0.0861
	C(2)	-0.0770	-0.0796	-0.0859
	C(3)	-0.1338	-0.1036	-0.1126
	C(4)	0.0550	0.0396	0.0267
	C(5)	0.0189	0.0440	0.0258
	C(6)	-0.0892	-0.1062	-0.1110
	C(7)	0.3444	0.3525	0.3405
	C(8)	0.0299	0.0182	0.0284
	C(9)	0.0446	0.0425	0.0308
	C(10)	0.3444	0.3520	0.3473
	C(11)	-0.1068	-0.1042	-0.1095
	C(12)	-0.0742	-0.0745	-0.0923
	C(13)	-0.1154	-0.1409	-0.1450
	C(14)	-0.1316	-0.1223	-0.1207
	O(15)	-0.4872	-0.4808	-0.4862
	O(16)	-0.4699	-0.4751	-0.5066
	S(17)	1.0872	1.1230	1.1212
	O(18)	-0.5407	-0.4052	-0.5894
	O(19)	-0.5142	-0.4744	-0.6018
	O(20)	-0.6854	-0.5971	-0.6071
	X(21)	0.7327 (Na)	0.3334 (H)	-
TNC		-3.5166	-3.2445	-3.6542
TNC/*n*		-0.1256	-0.1159	-0.1305

Frontier orbital energies and molecular electrostatic potential

Computational chemistry uses the highest occupied molecular orbital (HOMO) and the lowest unoccupied molecular orbital (LUMO) energies to predict the reactivity of molecules according to the frontier molecular orbital (FMO) theory. This approach allows for screening potential reactants and designing new molecules with desired reactivity profiles. The energies of HOMO and LUMO help identify the sites within a molecule that are most susceptible to electrophilic and nucleophilic attacks. In corrosion science, the HOMO and LUMO energies help in understanding the corrosion mechanism and inhibiting potential of compounds [39].

The FMO density distribution and molecular electrostatic potential (MEP) of different forms of the inhibitor molecule are presented in Figure 10.

The HOMO energy indicates the molecule's ability to donate electrons. The LUMO energy, in turn, represents the energy of the lowest occupied molecular orbital, indicating the molecule's ability to accept electrons. Molecules with higher E_{HOMO} and lower E_{LUMO} values can interact more effectively with the metal surface, enhancing their inhibition efficiency. The difference between HOMO and LUMO energies (energy gap, ΔE_{gap}) is an indicator of the stability and reactivity of inhibitors because electrons can be more easily excited from the HOMO to the LUMO, facilitating chemical reactions. A smaller ΔE_{gap} often indicates higher chemical reactivity, making the molecule more effective as a corrosion inhibitor. It also implies that the molecule can form a more stable adsorbed layer on the metal surface, providing better protection against corrosion. The calculated values of the HOMO, LUMO and ΔE energies indicate that the $AQ2S^-$ anion demonstrates the best inhibitory activity.

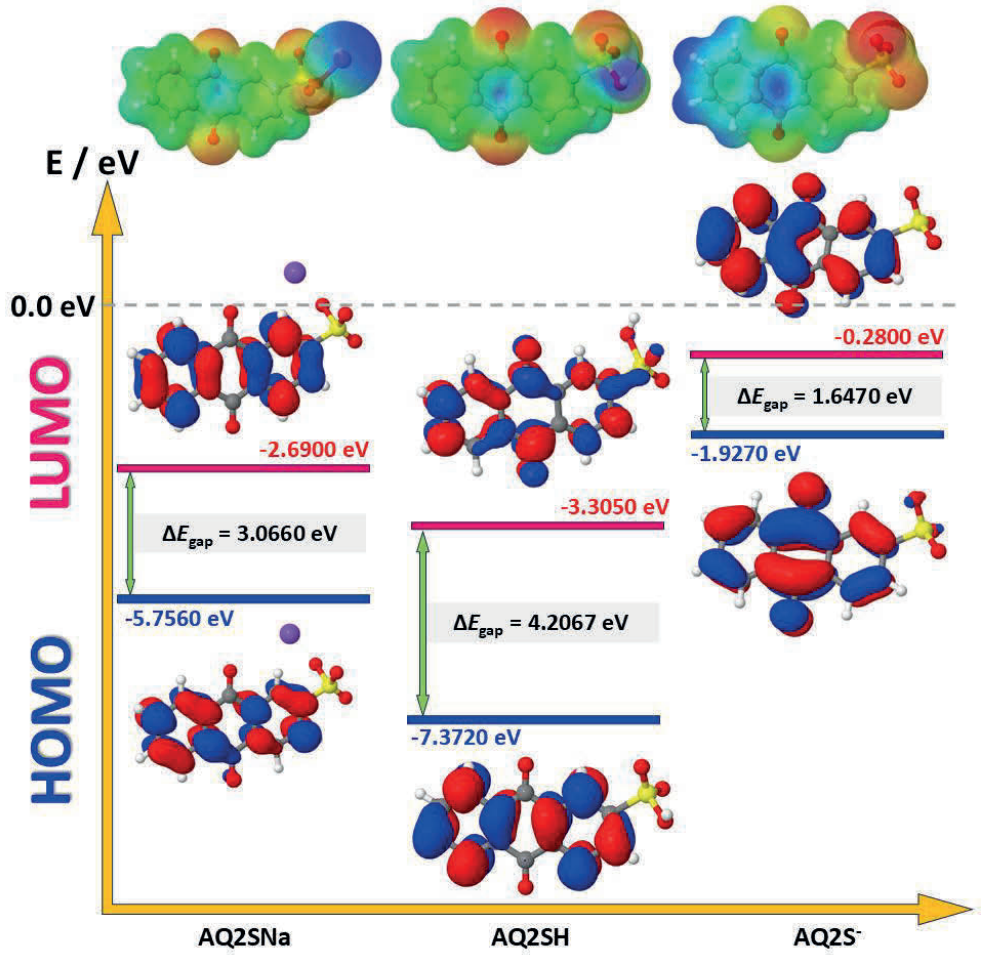

Figure 10. *HOMO, LUMO energies and density distribution, energy gap (ΔE_{gap}), and MEP for AQ2SNa, AQ2SH, and $AQ2S^-$*

Molecular reactivity

Quantum chemical descriptors provide rich details about molecules' electronic structure and properties, which are crucial for understanding and predicting molecular reactivity. These descriptors are used in combination with experimental data to explain the experimental results or predict the inhibition efficiency of new compounds.

Quantum chemical descriptors calculated for the inhibitor molecule in the form of sodium salt, acid and sulphonic anion are listed in Table 6.

In corrosion research, electron affinity (EA) and ionization potential (IP) are used to evaluate the tendency of a molecule to gain or lose electrons, which is critical for understanding the interaction of inhibitor molecules with the metal surface. A higher EA means the molecule can effectively accept electrons from the metal surface to form a stable adsorbed layer that protects against corrosion. According to the calculations, AQ2SH has the highest value of EA (3.3050 eV) and, therefore, should have the best inhibitory properties. The IP is directly correlated with the efficiency of corrosion inhibitors. Molecules with lower IP values tend to have higher inhibition efficiencies because they can more readily interact with the metal surface, forming a stable adsorbed layer that prevents corrosion. The ironic form of the inhibitor has the lowest value of IP and, therefore, should also have the best inhibitory properties.

Electronegativity (χ) and global hardness (η) provide an understanding of the electron-donating and accepting abilities of inhibitors.

Table 6. *Calculated reactivity descriptors for different forms of AQ2SNa in aqueous phase*

Descriptor	Formula	AQ2SNa	AQ2SH	$AQ2S^-$
Ionization energy (IP), eV	$IP = - E_{HOMO}$	5.7560	7.3720	1.9270
Electron affinity (EA), eV	$EA = - E_{LUMO}$	2.6900	3.3050	0.2800
Electronegativity (χ), eV	$\chi = \frac{I + A}{2}$	4.2230	5.3385	1.1035
Chemical hardness (η), eV	$\eta = \frac{I - A}{2}$	1.5330	2.0335	0.8235
Chemical softness (σ), eV	$\sigma = \frac{1}{\eta}$	0.6520	0.4917	1.2143
Electrophilicity index (ω), eV	$\omega = \frac{\chi^2}{2}$	0.7665	1.0167	0.4117
Nucleophilicity index (ε), eV	$\varepsilon = \frac{1}{\omega}$	1.3040	0.9835	2.4286
Back-donation energy ($E_{b\text{-}d}$, eV)	$\Delta E_{b\text{-}d} = -\frac{\eta}{4}$	-0.3830	-0.5083	-0.2058
Fraction of transferred electrons (ΔN)	$\Delta N = \frac{\chi_{Fe} - \chi_{inhibitor}}{2(\eta_{Fe} - \eta_{inhibitor})}$	0.5951	0.4533	0.9690

Higher electronegativity and lower hardness are generally associated with better inhibition performance. Inhibitors with high electronegativity are better at accepting electrons from the metal surface, which can help in forming a protective layer. Global hardness is a measure of a molecule's resistance to the deformation of its electron cloud. Higher η indicates greater stability and lower reactivity, which can be beneficial for inhibitors as they are less likely to undergo unwanted chemical reactions. Global softness (σ), in turn, is the inverse of global hardness and measures the ease with which a molecule's electron cloud can be deformed. Higher global softness indicates higher reactivity, which can be advantageous for inhibitors as they can more easily interact with the metal surface to form a protective layer. Soft molecules are more polarizable and can form stronger interactions with the metal surface, leading to better adsorption and inhibition efficiency. A higher global softness

indicates that the molecule is more reactive and can easily interact with the metal surface, enhancing its corrosion inhibition properties. The calculation results show that the acidic form of the inhibitor molecule has the highest electronegativity. However, the ionic form has the lowest hardness and the highest softness values, indicating its increased anticorrosive activity compared with other forms of the inhibitor molecule. Electrophilicity (ω) and nucleophilicity (ε) indexes are also important quantum chemical descriptors that provide insights into the properties and effectiveness of corrosion inhibitors. A higher electrophilicity index indicates a greater ability to accept electrons, making the molecule more reactive towards electron-rich sites on the metal surface. The nucleophilicity index (ε) is a parameter reciprocal to the electrophilicity index, which is used to describe the ability of a molecule to donate electrons. Corrosion inhibitors with higher nucleophilicity indices are generally more effective because they can more readily form bonds with the metal surface. High values of this parameter are typical for inhibitors with heteroatoms like nitrogen, oxygen, and sulfur, which are known for their electron-donating properties. According to the calculated results, the ionic form of the inhibitor molecule has the highest nucleophilicity index, which also confirms its tendency to exhibit high inhibitory properties. Back-donation energy ($E_{b\text{-}d}$) in conjunction with electrophilicity and nucleophilicity indexes provides a comprehensive understanding of the inhibitor's reactivity and interaction with the metal surface. Back-donation energy refers to the energy change associated with the transfer of electrons from the metal surface back to the inhibitor molecule. A significant back-donation energy indicates a strong interaction between the inhibitor and the metal surface and the stability of the adsorbed layer. The ionic form of the AQ2SNa has the highest value of back-donation energy (-0.2058), which clearly indicates its significant inhibitory properties. The fraction of transferred electrons (ΔN) represents the number of electrons transferred from the inhibitor molecule to the metal surface. A higher Δ*N* value generally indicates a stronger interaction between the inhibitor and the metal, leading to better corrosion inhibition efficiency. A positive ΔN suggests that electron transfer occurs from the inhibitor to the metal, which helps in passivating the metal surface and preventing corrosion. The Δ*N* values calculated for all forms of the inhibitor are positive. At the same time, the highest value is characteristic of the ionic form (0.9690 eV), which indicates its greater tendency to transfer electrons to the metal surface and thereby also confirms its more significant inhibitory effectiveness.

The obtained calculation results show that the ionic form of the inhibitor molecule ($AQ2S^-$) has higher inhibitory properties. The electron-donating ability is most pronounced for this form, contributing to its greater tendency to adsorb on the metal surface and forming a strong protective layer.

Molecular dynamic simulation and adsorption energy

The interaction between the active sites of different forms of the inhibitor and Fe (110) surface was explained using MD simulation. A deeper understanding of the interaction between each form of the inhibitor and Fe (110) metal surface was gained through MD simulation. The lowest energy configurations of different forms of the inhibitor in the simulated system are presented in Figure 11.

As can be seen, the inhibitor adsorbs in its anion form, lying flat on the Fe(110) surface. Acidic and salt forms of the inhibitor molecule are exhibited at an angle to the metal surface. This spatial arrangement of the inhibitor molecules is in excellent agreement with the results of quantum chemical calculations, in particular with the MACD and MEP. According to MACD, the flat-lying adsorption geometries suggest that this process is supported through oxygen atoms of both functional groups of the inhibitor molecule.

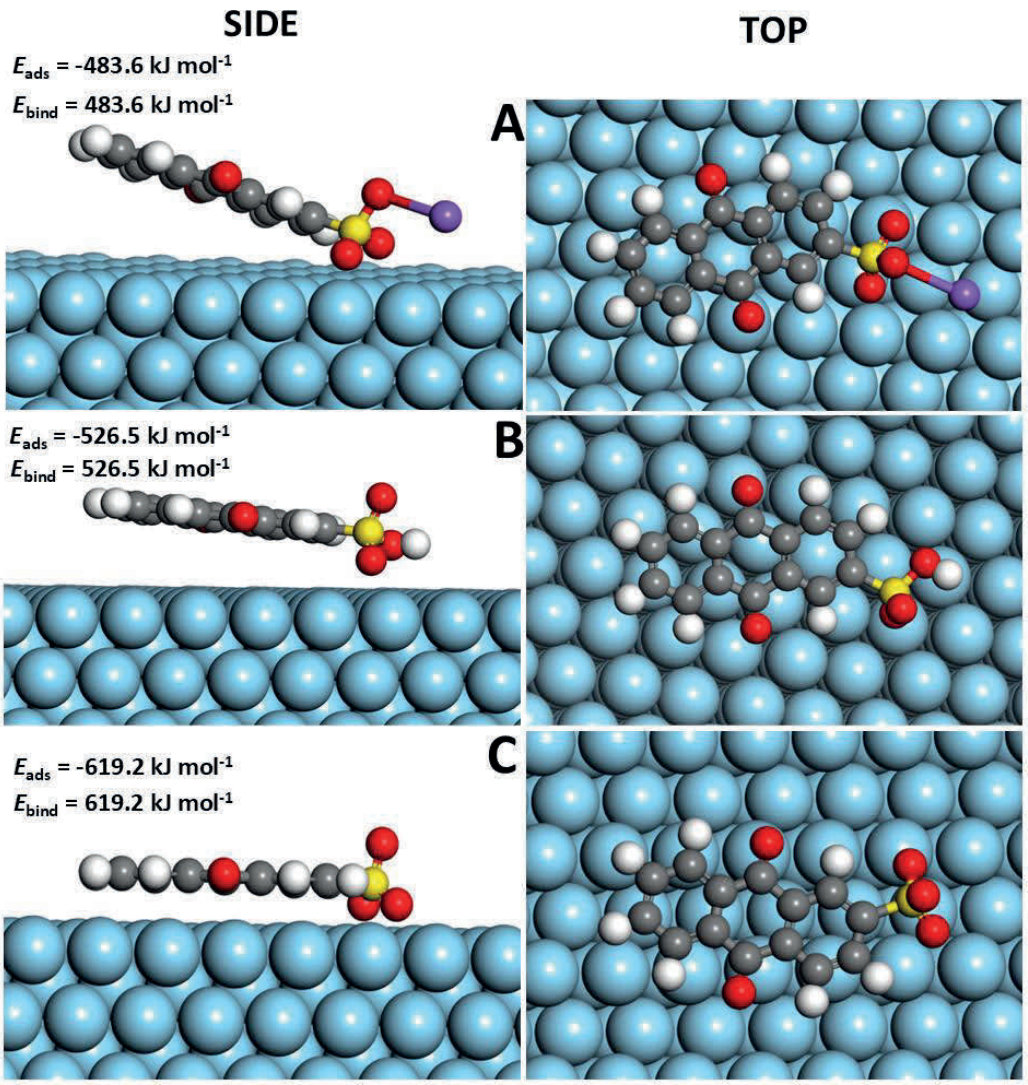

Figure 11. *Side and top views of the most appropriate configuration for adsorption of AQ2SNa (A), AQ2SH (B), and AQ2S$^-$ molecules (C) on the Fe (110) surface obtained by MD simulations in aqueous solution (water molecules were removed for clarity)*

A more negative and evenly distributed charge on the oxygen atoms of the carbonyl groups in the anion contributes to a flatter arrangement of the molecule from the metal surface. In all three forms, the inhibitor molecules are adsorbed on a metal surface primarily due to two oxygen atoms of the sulfo group, since these atoms have the most negative charge. Binding energy quantifies the strength of the interaction between the inhibitor and the metal, providing insights into the stability of the adsorbed layer. The sorption and binding energy values clearly show that the anionic form sorbs better on the metal surface. Thus, it can be inferred that the inhibitor molecules adsorb on the metal surface to form a dense molecular layer, separating the metal surface from the water molecules to achieve the effect of corrosion inhibition.

Adsorption and corrosion inhibition mechanism

From the obtained experimental and theoretical results, we propose the adsorption mechanism presented in Figure 12. The results clearly show that the inhibitor adsorbs on the metal surface as a sulfonate anion. The inhibitor molecules bind to the negatively charged metal surface through attractive electrostatic forces. In parallel, the lone electron pairs of the oxygen atoms of the -C=O and -SO_3^- moieties and the π-electrons of the aromatic rings donate electrons to the vacant *d*-orbitals of the Fe atoms, which leads to the chemisorption.

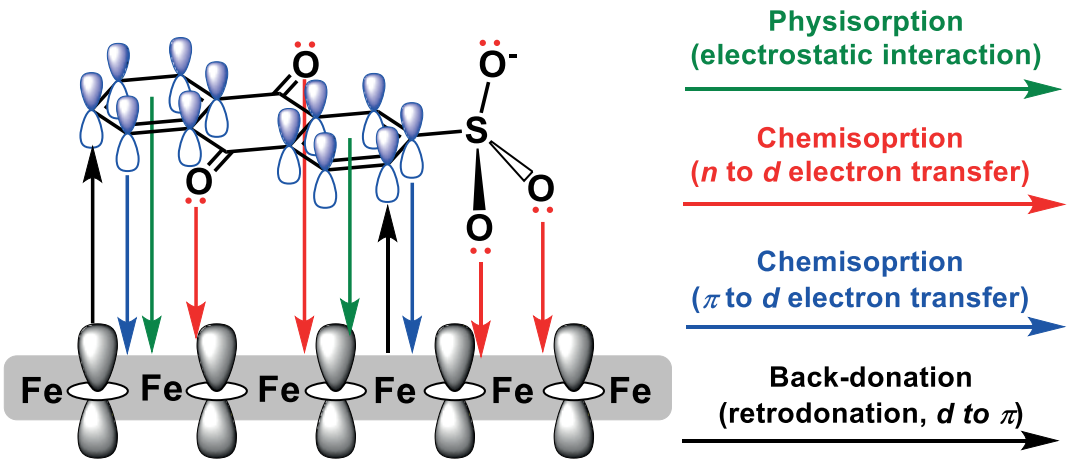

Figure 12. *Representation of adsorption mechanism of AQ2S⁻ on Fe(110) surface*

This transfer leads to the accumulation of electrons in the *d*-orbitals of the metal atoms, resulting in inter-electron repulsions. In order to avoid this repulsion phenomenon, a reverse transfer of electrons takes place from the *d*-orbitals of the surface metal atoms to the unoccupied molecular orbitals of the inhibitor molecules (retro-donation), thus reinforcing the adsorption of the inhibitor molecules on the metal surface.

It can be concluded that adsorption of the inhibitor on the Fe (110) surface in an acidic solution occurs through physisorption, chemisorption and retro-donation. In addition, theoretical studies show a good correlation with electrochemical studies, which show that AQ2SNa has high corrosion inhibition performance.

Conclusions

This study investigated the potential of AQ2SNa as a corrosion inhibitor on carbon steel in 0.5 mol dm^{-3} H_2SO_4 solution experimentally and theoretically. AQ2SNa showed significant inhibitory properties against the corrosion of carbon steel in a given medium. The maximum protection efficiency of the metal reaches up to 94.44 % at 333 K and an inhibitor concentration of 0.5 g dm^{-3}. The adsorption of the inhibitor on the metal surface adheres to the Langmuir model. The protective film is formed due to spontaneous physisorption by creating a physical barrier between the metal surface and the corrosive environment. The inhibitor exhibits mixed-type properties, mainly reducing the rate of the cathodic process. An increase in the temperature and concentration of the inhibitor positively affects the anticorrosive performance of AQ2SNa. The increasing temperature and concentration of the inhibitor induce a significantly proportional increase in its protective effect. The data from the electrochemical experiments are in complete agreement with the results of the gravimetric measurements. An increase in polarization resistance and a decrease in corrosion current indicate a hindrance to the corrosion process in the presence of AQ2SNa. These suggest a robust protective layer forms on the metal surface, enhancing its resistance to acidic corrosive agents. Gravimetric and electrochemical results were rationalized by theoretical methods. The density functional theory calculations predicted that $AQ2S^-$ ion is a real corrosion inhibitor in a model system with O atoms as the most possible adsorption centers. Moreover, the MD simulation revealed the strong adsorption interaction of $AQ2S^-$ towards the Fe (110) surface. The obtained theoretical results are in agreement with the experimental ones. Thus, AQ2SNa is an effective inhibitor for corrosion protection of carbon steel in 0.5 mol dm^{-3} H_2SO_4 solution. The results of this study open up new prospects for the further application of this useful compound for anticorrosive protection of metals in acidic environments.

References

[1] A. F. Hamood, H. S. Aljibori, M. A. I. Al-Hamid, A. A. Alamiery, W. K. Al-Azzawi, MOP as a Corrosion Inhibitor for Mild Steel in HCl Solution, A Comprehensive Study, *The Progress in Color, Colorants and Coatings* **17** (2024) 207-226. https://doi.org/10.30509/pccc.2023.16θ7176.1237

[2] T. Seilova, Z. Kunasheva, R. Kubasheva, N. Akatyev, Development of new three-component BNP-inhibitor for carbon steel in 0.5 mol dm^{-3} HCl solution, Thermodynamic, adsorption and electrochemical studies, *The International Journal of Corrosion and Scale Inhibition* **13** (2024) 1268-1291. http://dx.doi.org/10.17675/2305-6894-2024-13-2-33

[3] H. Bairagi, P. Vashishth, G. Ji, S.K. Shukla, E. E. Ebenso, B. Mangla, Polymers and their composites for corrosion inhibition application: development, advancement, and future scope - a critical review, *Corrosion Communications* **15** (2024) 79-94. https://doi.org/10.1016/j.corcom.2023.10.006

[4] M. Sheydaei, The Use of Plant Extracts as Green Corrosion Inhibitors: A Review, *Surfaces* **7** (2024) 380-403. http://dx.doi.org/10.3390/surfaces7020024

[5] Q. Wang, R. Wang, Q. Zhang, C. Zhao, X. Zhou, H. Zheng, R. Zhang, Y. Sun, Z. Yan, Application of biomass corrosion inhibitors in metal corrosion control: a review, *Molecules* **28** (2023) 2832. http://dx.doi.org/10.3390/molecules28062832

[6] G. Ji, Waste natural materials for sustainable corrosion prevention of steel: A mini review on their popularity, experimental and computational investigation, applications, challenges, and future strategy, *Journal of Molecular Liquids* **408** (2024) 125415 https://doi.org/10.1016/j.molliq.2024.125415

[7] I. Pandey, A. V. Ullas, C. K. Rastogi, M. K. Singh, V. Kumar, B. Mangla, G. Ji, Extract Preparation of Waste Lady Finger Caps Using Ethanol, Generation of Extract's Layers on Copper Through Drop Casting Without and with NiO Nanoparticles, and Study of their Corrosion Performances in Saline Water, *Waste and Biomass Valorization* (2024). https://doi.org/10.1007/s12649-024-02729-4

[8] S.B. Ade, Corrosion inhibition of mild steel in different acid medium by using various acidic groups of organic compounds, *International Journal for Research in Applied Science and Engineering Technology* **10** (2022) 367-373. http://dx.doi.org/10.22214/ijraset.2022.40288

[9] A. N. Kuzyukov, I. A. Levin, Effect of anthraquinone and some of its derivatives on the corrosion resistance of metals in sulfuric acid solutions, *Chemical and Petroleum Engineering* **5** (1969) 787-788. https://doi.org/10.1007/BF01153172

[10] N. Muthukumar, A. Ilangovan, S. Maruthamuthu, N. Palaniswamy, A. Kimura, 1 - Aminoanthraquinone derivatives as a novel corrosion inhibitor for carbon steel API 5L-X60 in white petrol–water mixtures, *Materials Chemistry and Physics* **115 (1) (**2009) 444-452. https://doi.org/10.1016/J.MATCHEMPHYS.2008.12.027

[11] L. Saqalli, M. Galai, N. Gharda, M. Sahrane, R. Ghailane, M. Ebn Touhami, Y. Peres-lucchese, A. Souizi, N. Habbadi, Corrosion inhibition of carbon steel by anthraquinones derivatives in 1.0 M HCl: Electrochemical and quantum calculations, *International Journal of Electrochemical Science* **13(5)** (2018) 5096-5119. https://doi.org/10.20964/2018.05.40

[12] L. Saqalli, M. Galai, F. Benhiba, N. Gharda, N. Habbadi, R.Ghailane, M. Ebn Touhami, Y. Peres-lucchese, A. Souizi, R. Touir, Experimental and theoretical studies of Alizarin as corrosion inhibitor for mild steel in 1.0 M HCl solution. *Journal of Materials and Environmental Science* **8** (2017) 2455-2467. https://www.jmaterenvironsci.com/Document/vol8/vol8_N7/264-JMES-2627-Saqalli.pdf

[13] Z. Bensouda, M. Driouch, M. Sfaira, A. Farah, M. Ebn Touhami, B. Hammouti, K. M. Emran, Effect of *Mentha Piperita* essential oil on mild steel corrosion in hydrochloric acid,

International Journal of Electrochemical Science **13** (2018) 8198-8221. https://doi.org/10.20964/2018.08.79

[14] X. Miao, X. Zhang, S. Chen, Y. Liu, Y. Chen, J. Lin, Y. Zhang, Dual-redox enhanced supercapacitors with sodium anthraquinone-2-sulfonate and potassium bromide, *Electrochimica Acta* **374** (2021) 137889. https://doi.org/10.1016/j.electacta.2021.137889

[15] P. R. Maddigapu, A. Bedini, C. Minero, V. Maurino, D. Vione, M. Brigante, M. Sarakha, The pH-dependent photochemistry of anthraquinone-2-sulfonate, *Photochemical & Photobiological Sciences* **9** (2010) 323. https://doi.org/10.1039/b9pp00103d

[16] A. V. Losub, S. S. Stahl, Palladium-Catalyzed Aerobic Oxidative Dehydrogenation of Cyclohexenes to Substituted Arene Derivatives, *Journal of the American Chemical Society*, **137** (2015) 3454-3457. https://doi.org/10.1021/ja512770u

[17] L. Zhang, P. Chen, Y. Xu, W. Nie, Y. Zhou, Enhanced photo-induced antibacterial application of graphene oxide modified by sodium anthraquinone-2-sulfonate under visible light, *Applied Catalysis B: Environmental* **265** (2020) 118572. https://doi.org/10.1016/j.apcatb.2019.118572

[18] S.Khankaew, A. Mills, D. Yusufu, N. Wells, S. Hodgen, W. Boonsupthip, P. Suppakul, Multifunctional anthraquinone-based sensors: UV, O_2 and time, *Sensors and Actuators B: Chemical* **238** (2017) 76-82. http://dx.doi.org/10.1016/j.snb.2016.07.037

[19] R. Sun, D. Han, C. Cui, Z. Han, X. Guo, B. Zhang, Y. Guo, Y. Liu, Z. Weng, Q.-H. Yang, A Self-Deoxidizing Electrolyte Additive Enables Highly Stable Aqueous Zinc Batteries, *Angewandte Chemie International Edition* **62** (2023) e202303557. https://doi.org/10.1002/anie.202303557

[20] L. Zhang, J. Huang, H. Guo, L. Ge, Z. Tian, M. Zhang, J. Wang, G. He, T. Liu, J. Hofkens, D.J.L. Brett, F. Lai, Tuning Ion Transport at the Anode-Electrolyte Interface via a Sulfonate-Rich Ion-Exchange Layer for Durable Zinc-Iodine Batteries, *Advanced Energy Materials* **13** (2023) 2203790. http://dx.doi.org/10.1002/aenm.202203790

[21] ISO 8407-2021: Corrosion of metals and alloys - Removal of corrosion products from corrosion test specimens (2021). Geneva, Switzerland.

[22] L. T. Popoola, Organic green corrosion inhibitors (OGCIs): a critical review, *Corrosion Reviews* **37(2)** (2019) 71-102. https://doi.org/10.1515/corrrev-2018-0058

[23] Ya. G. Avdeev, Yu. I. Kuznetsov, Chemical transformation of corrosion inhibitors in the aggressive environment/metal system, *International Journal of Corrosion and Scale Inhibition* **12(4)** (2023) 1751-1790. https://dx.doi.org/10.17675/2305-6894-2023-12-4-19

[24] C. G. Zhan, J. A. Nichols, D. A. Dixon, Ionization potential, electron affinity, electronegativity, hardness, and electron excitation energy: molecular properties from density functional theory orbital energies, *The Journal of Physical Chemistry A* **107(20)** (2003) 4184-4195. https://doi.org/10.1021/jp0225774

[25] M. W. Schmidt, K. K. Baldridge, J. A. Boatz, S. T. Elbert, M. S. Gordon, J. H. Jensen, S. Koseki, N. Matsunaga, K. A. Nguyen, S. Su, T. L. Windus, M. Dupuis, J. A. Montgomery Jr, General atomic and molecular electronic structure system, *Journal of computational chemistry* **14(11)** (1993) 1347-1363. https://doi.org/10.1002/jcc.540141112

[26] A. Klamt, The COSMO and COSMO-RS solvation models, WIREs Computational Molecular Science **8(1)** (2017) e1338. https://doi.org/10.1002/wcms.1338

[27] M. J. Abraham, T. Murtola, R. Schulz, S. Pall, J. C. Smith, B. Hessa, E. Lindahl, GROMACS: High performance molecular simulations through multi-level parallelism from laptops to supercomputers, *SoftwareX* **1** (2015) 19-25. https://doi.org/10.1016/j.softx.2015.06.001

[28] N. Mazlan, K. Jumbri, M. A. Kassim, R. A. Wahab, M. B. A. Rahman, Density functional theory and molecular dynamics simulation studies of bio-based fatty hydrazide-corrosion inhibitors

on Fe (110) in acidic media, *Journal of Molecular Liquids* **347(1)** (2022) 118321. https://doi.org/10.1016/j.molliq.2021.118321

[29] M. Husaini, M.B. Ibrahim, Thermodynamic and Kinetic study on the corrosion, of aluminium in hydrochloric acid using benzaldehyde as corrosion inhibitor, *International Journal of Engineering and Manufacturing* **9(6)** (2019) 53-64. https://doi.org/10.5815/ijem.2019.06.05

[30] L. Afia, R. Salghi, A. Zarrouk, H. Zarrok, O. Benali, B. Hammouti, S. S. Al-Deyab, A. Chakir, L. Bazzih, Inhibitive action of argan press cake extract on the corrosion of steel in acidic media, *Portugaliae Electrochimica Acta* **30(4)** (2012) 267-279. https://doi.org/10.4152/PEA.201204267

[31] A. A. Khadom, A. S. Yaro, H. A. A. Kadum, A. S. AlTaie, A. Y. Musa, The Effect of Temperature and Acid Concentration on Corrosion of Low Carbon Steel in Hydrochloric Acid Media, *American Journal of Applied Sciences* **6(7)** (2009) 1403-1409. https://doi.org/10.3844/ajassp.2009.1403.1409

[32] J. Sirajudeen, M. M. Mohamed Mubashir, Statistical approach and assessment of physico-chemical status of ground water in near proximity of South Bank Canal, Tamil Nadu, India, *Archives of Applied Science Research* **5(2)** (2013) 25-32.

[33] A. A. Khadom, A. S. Yaro, A. A. H. Kadhum, Adsorption Mechanism of Benzotriazole for Corrosion Inhibition of Copper-Nickel Alloy in Hydrochloric Acid, *Journal of the Chilean Chemical Society* **55(1)** (2010) 150-152. https://doi.org/10.4067/s0717-97072010000100035

[34] N. Mohanapriya, M. Kumaravel, B. Lalithamani, Theoretical and experimental studies on the adsorption of n-[(E)-pyridin-2-ylmethylidene] aniline, a Schiff base, on mild steel surface in acid media, *Journal of Electrochemical Science and Technology* **11(2)** (2020) 117-131. https://doi.org/10.33961/jecst.2019.00430

[35] A. S. Fouda, H. E. Megahed, N. Fouad, N. M. Elbahrawi, Corrosion inhibition of carbon steel in 1 M hydrochloric acid solution by aqueous extract of *Thevetia peruviana*, *Journal of Bio- and Tribo-Corrosion* **2** (2016) 16. https://doi.org/10.1007/s40735-016-0046-z

[36] M. Husaini, M. B. Ibrahim, Investigation of inhibition potential effect of organic compound for the corrosivity of phosphoric acid on aluminium, *International Journal of Engineering and Manufacturing* **10(1)** (2020) 41-53. https://doi.org/10.5815/ijem.2020.01.04

[37] R. Solmaz, G. Kardaş, B. Yazıcı, M. Erbil, Adsorption and corrosion inhibitive properties of 2-amino-5-mercapto-1, 3, 4-thiadiazole on mild steel in hydrochloric acid media, *Colloids and Surfaces A: Physicochemical and Engineering Aspects* **312(1)** (2008) 7-17. https://doi.org/10.1016/j.colsurfa.2007.06.035

[38] El S. H. El Ashry, A. El Nem, S. A. Essawy, S. Ragab, Corrosion inhibitors, part 31: quantum chemical studies on the efficiencies of some aromatic hydrazides and Schiff bases as corrosion inhibitors of steel in acidic medium, *Arkivoc* **11** (2006) 205-220. https://doi.org/10.3998/ARK.5550190.0007.B21

[39] P. Dhakal, W. Gassaway, J. K. Shah, Mapping the frontier orbital energies of imidazolium-based cations using machine learning, *The Journal of Chemical Physics* **159** (2023) 064513. https://doi.org/10.1063/5.0155775